Am J Physiol Endocrinol Metab 310: E515–E525, 2016.
First published January 19, 2016; doi:10.1152/ajpendo.00500.2015.

Is bursting more effective than spiking in evoking pituitary hormone secretion? A spatiotemporal simulation study of calcium and granule dynamics

Alessia Tagliavini,[1] Joël Tabak,[2,3] Richard Bertram,[2] and Morten Gram Pedersen[1]

[1]*Department of Information Engineering, University of Padua, Padua, Italy;* [2]*Department of Mathematics and Program in Neuroscience and Molecular Biophysics, Florida State University, Tallahassee, Florida; and* [3]*Exeter University Medical School, Biomedical Neuroscience, Exeter, United Kingdom*

Submitted 25 November 2015; accepted in final form 12 January 2016

Tagliavini A, Tabak J, Bertram R, Pedersen MG. Is bursting more effective than spiking in evoking pituitary hormone secretion? A spatiotemporal simulation study of calcium and granule dynamics. *Am J Physiol Endocrinol Metab* 310: E515–E525, 2016. First published January 19, 2016; doi:10.1152/ajpendo.00500.2015.—Endocrine cells of the pituitary gland secrete a number of hormones, and the amount of hormone released by a cell is controlled in large part by the cell's electrical activity and subsequent Ca^{2+} influx. Typical electrical behaviors of pituitary cells include continuous spiking and so-called pseudo-plateau bursting. It has been shown that the amplitude of Ca^{2+} fluctuations is greater in bursting cells, leading to the hypothesis that bursting cells release more hormone than spiking cells. In this work, we apply computer simulations to test this hypothesis. We use experimental recordings of electrical activity as input to mathematical models of Ca^{2+} channel activity, buffered Ca^{2+} diffusion, and Ca^{2+}-driven exocytosis. To compare the efficacy of spiking and bursting on the same cell, we pharmacologically block the large-conductance potassium (BK) current from a bursting cell or add a BK current to a spiking cell via dynamic clamp. We find that bursting is generally at least as effective as spiking at evoking hormone release and is often considerably more effective, even when normalizing to Ca^{2+} influx. Our hybrid experimental/modeling approach confirms that adding a BK-type K^+ current, which is typically associated with decreased cell activity and reduced secretion, can actually produce an increase in hormone secretion, as suggested earlier.

electrical activity; exocytosis; Ca^{2+} oscillations; mathematical modeling; dynamic clamp

ENDOCRINE CELLS OF THE PITUITARY GLAND (i.e., melanotrophs, lactotrophs, somatotrophs, thyrotrophs, corticotrophs, and gonadotrophs) secrete a number of hormones and are regulated by the hypothalamus (30). These hormones act on other endocrine glands and other tissues, including the brain, to regulate physiological and behavioral aspects of growth, metabolism, water balance, and reproduction (7). The endocrine pituitary cells contain a wide variety of ion channels and are electrically excitable, and hormone secretion occurs due to an elevation in the intracellular Ca^{2+} concentration that often accompanies electrical activity (29). Common behaviors of the cells include continuous spiking, typically observed in luteinizing hormone-secreting gonadotrophs under basal conditions, and a form of bursting known as pseudo-plateau bursting that is often observed in prolactin-secreting lactotrophs, growth hormone-releasing somatotrophs, and ACTH-secreting corticotrophs, where the burst duration is at most a few seconds and the spikes that ride on the elevated voltage plateau are very small (9, 10). Each electrical event brings Ca^{2+} into the cell, and this Ca^{2+} is responsible for exocytosis of hormone-filled granules. Simultaneous measurements of both electrical activity and Ca^{2+} concentration have established that the amplitude of Ca^{2+} fluctuations is greater in a bursting cell than in a spiking cell (30), leading to the hypothesis that bursting cells release more hormones than spiking cells (8, 9). Experimentally exploring this hypothesis will require simultaneous measurements of electrical activity and release from single cells. The aim of this report is to use computer simulations to explore the hypothesis that pseudo-plateau bursting evokes more secretion than continuous spiking.

The approach that we use is to directly measure electrical spiking and bursting patterns from pituitary cells and use these data as input to mathematical models of Ca^{2+} channel activity, Ca^{2+} diffusion and binding to buffer, and finally, Ca^{2+}-driven exocytosis Table 1. The model parameters are set according to prior data and models, but one major unknown factor is the geometrical arrangement of Ca^{2+} channels and docked granules at the plasma membrane. We consider the secretion response to stochastic single channels as well as small clusters of stochastic channels and vary the distance of the channels from the release sites. Our objective was to determine how these factors affect the differential secretion evoked by spiking electrical activity vs. bursting electrical activity.

We find that bursting is typically more effective at evoking secretion than is continuous spiking. When bursting is induced in a spiking gonadotroph by injecting a large-conductance potassium (BK)-type K^+ current with dynamic clamp, our model simulations suggest that the burst pattern is generally at least as effective as continuous spiking at evoking hormone release and is often considerably more effective. We demonstrate that the degree of superiority of bursting over spiking depends on the channel configuration, which would likely vary from cell to cell. We also demonstrate that the bursting reappearing in an endogenously bursting pituitary cell, after previously pharmacologically blocking the native BK current and subsequently adding a BK current using dynamic clamp, is superior at evoking secretion than the pharmacologically induced spiking behavior. Thus, we demonstrate with this hybrid experimental/modeling approach that adding a K^+ current, which is typically associated with decreased cell activity and reduced secretion, can actually produce an increase in hormone secretion, as suggested earlier (9).

Address for reprint requests and other correspondence: M. G. Pedersen, Dept. of Information Engineering, Univ. of Padua, Via Gradenigo 6/B, 35131 Padua, Italy (e-mail: pedersen@dei.unipd.it).

Table 1. *Default parameters of the Ca^{2+} channel model, Ca^{2+} diffusion simulations, and exocytosis model*

Parameter	Value	Unit
Current simulation		
s_m	7	mV
v_m	−4	mV
k_+	0.0234	ms^{-1}
k_-	0.018	ms^{-1}
g_{Ca}	20	pS
Diffusion simulation		
D_{Ca}	0.22	$\mu m^2\ s^{-1}$
B_{total}	900	μM
K_D	10	μM
k_{on}	0.1	$\mu M^{-1}\ ms^{-1}$
k_{off}	1	ms^{-1}
$[Ca^{2+}]_0$	0.22	μM
Secretion model		
k_1	3.7	$\mu M^{-1}\ s^{-1}$
k_{-1}	100	s^{-1}
r_1^0	3.6	s^{-1}
K_p	2.3	μM
r_{-1}	0.001	s^{-1}
u_1	1,000	s^{-1}

METHODS

The inputs to our mathematical models are voltage time courses recorded from a rat gonadotroph or from a GH4C1 lacto-somatotroph cell. We used traces consisting of continuous spiking patterns and traces of fast pseudo-plateau bursting caused by adding a BK-type current to a spiking cell with the dynamic clamp technique. Each of these traces was fed into a mathematical model consisting of stochastic Ca^{2+} channels coupled to reaction-diffusion equations that describe Ca^{2+} transport through the cell. Finally, the computed Ca^{2+} concentration was used to drive an exocytosis model based on Ca^{2+} binding to granules, granule fusion with the membrane, and resulting hormone release.

Experiments

GH4C1 cells were maintained in culture conditions in supplemented F10 medium (Sigma-Aldrich, St. Louis, MO) according to established procedures (35). Primary pituitary cells were obtained from diestrous female rats (Sprague-Dawley, aged 3–6 mo) using enzymatic dispersion of pituitary fragments (33). Animal procedures were approved by the Florida State University Animal Care and Use Committee. Cells were cultured in supplemented M199 medium (Invitrogen, Carlsbad, CA) for 1 day before being used for patch clamp experiments. Gonadotrophs were identified by their larger size and by their typical rhythmic hyperpolarizations in response to 1 nM gonadotropin-releasing hormone (Bachem, Torrance, CA) applied at the end of the experiment (38).

During the patch clamp experiments, cells were superfused with HEPES-buffered saline (138 mM NaCl, 5 mM KCl, 10 mM D-glucose, 25 mM HEPES, 0.7 mM Na_2HPO_4, 1 mM $MgCl_2$, and 2 mM $CaCl_2$) at room temperature. Patch pipettes (resistance 6–9 MOhm) were filled with a solution containing 90 mM KAsp, 60 mM KCl, 10 mM HEPES, and 1 mM $MgCl_2$ with the addition of 120 g/ml amphotericin B. Usually, access resistance decreased below 50 MOhm within 10 min following seal (>5 GOhm) formation. BK channels were blocked by bath application of 100 nM iberiotoxin (Tocris).

Dynamic Clamp

Membrane potential was recorded in current clamp (bridge mode), and output from the patch amplifier (Multiclamp 700B; Molecular Devices, Sunnyvale, CA) was read through an analog-to-digital acquisition card on a PC running the software QuB with a dynamic clamp module (22). Membrane potential (V) was used to compute the current going through the BK channels, $I_{BK} = g_{BK}\, f\, (V_K - V)$, with f obtained by integrating

$$\tau_{BK}\frac{df}{dt} = f_\infty(V) - f \qquad (1)$$

in real time using the forward Euler method (22); dt average = 54 μs, maximum = 100 μs, and the steady-state BK channel activation is given by

$$f_\infty(V) = \left[1 + \exp\left((v_f - V)/s_f\right)\right]^{-1}. \qquad (2)$$

The calculated BK current was injected back into the cell through the same analog-to-digital acquisition card. The parameter values were $g_{BK} = 0.5 - 1$ nS, $\tau_{BK} = 5 - 10$ ms; $v_f = -15$ mV, and $s_f = 1$ mV.

Modeling

Geometry. To model data from pituitary cells, we represented a single cell by a sphere with a diameter of 13 μm (5). Based on whole cell calcium conductance of ~1.5–2 nS (10) and single-channel conductance ~20 pS (13), we assumed that a cell possesses 75 functional L-type Ca^{2+} channels. In our simulations we considered two different configurations for the channel distribution over the sphere surface; channels were either uniformly distributed, with each release site affected by a single channel, or there were clusters composed of five channels, with each release site affected by a single cluster. In the single-channel case, Ca^{2+} diffusion was computed in a conical region with base radius of 1.5 μm (Fig. 1*A*), a radius obtained by dividing the sphere surface into 75 circular areas, one for each channel. This radius corresponds to an interchannel distance of ~3 μm, in agreement with Hagiwara and Ohmori (11). The single-channel conductance was set to 20 pS (13). In the case of channel clusters, Ca^{2+} diffusion was simulated in a conical region with a base radius of 3.3 μm, corresponding to dividing the sphere surface into 15 circular areas. In both cases, the Ca^{2+} current source was located at the base center of the conical region. We implemented no-flux boundary conditions for Ca^{2+} and buffers on the sides of the cone. This assumption means that Ca^{2+} flowing out of the conical region equals the flux into the cone from adjacent regions, or in other words, the Ca^{2+} channels in adjacent cones contribute to Ca^{2+} levels in the cone of study exactly as the Ca^{2+} channel or cluster under study influences the adjacent regions. Because of the conical geometry, the full three-dimensional problem was reduced to a two-dimensional problem, using rotationally symmetric spherical (r, θ) coordinates, thus reducing the computational requirements. Since the granules participating in hormone secretion are located just below the membrane (14), we focused our attention on the submembrane Ca^{2+} profiles along the plasma membrane.

Single-channel current. For the single Ca^{2+} channel, we assumed three states with kinetic mechanism described by (28)

$$C \underset{\beta}{\overset{\alpha}{\rightleftarrows}} O \underset{k_-}{\overset{k_+}{\rightleftarrows}} B \qquad (3)$$

where the states are closed (C), open (O), and blocked or inactivated (B).

The rate constants $\alpha(V)$ and $\beta(V)$ were determined by $\alpha = m_\infty/\tau_m$, $\beta = 1/\tau_m - \alpha$ (12) using a steady-state activation function m_∞ and time constant τ_m obtained from experiments. Based on data from GH3 cells (5, 11), which have Ca^{2+} channel characteristics similar to GH4 cells (5), and in agreement with Sherman et al. (28), we set τ_m at 1.25 ms. The steady-state activation function was

$$m_\infty = \frac{1}{1 + \exp\left[(V_m - V)/s_m\right]}, \qquad (4)$$

with $V_m = -4$ mV and $s_m = 7$ mV (11). With regard to channel inactivation, some types of Ca^{2+} channels are inactivated by Ca^{2+},

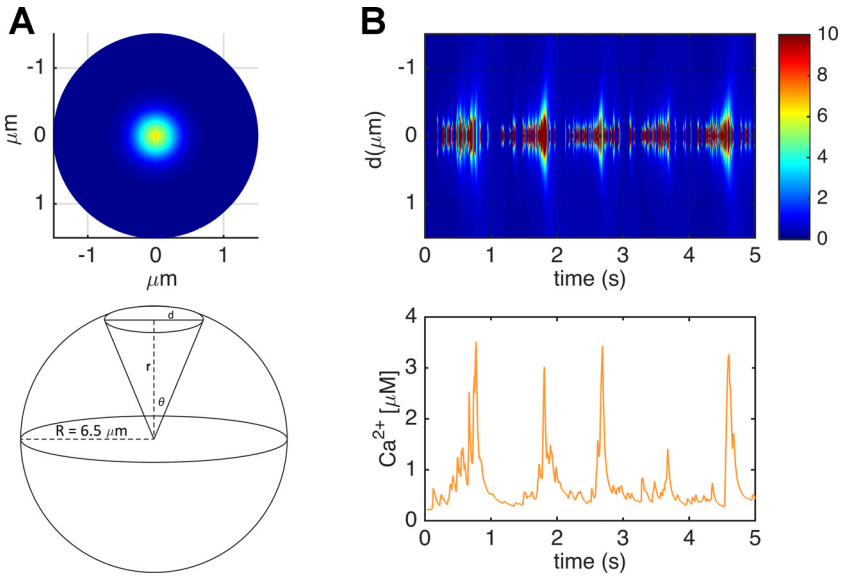

Fig. 1. Calcium diffusion characteristics in the model. *A*: spherical cell model used in simulations. The cell diameter is 13 μm. Ca^{2+} diffusion and buffering are simulated in a conical region of the sphere. The channel or channel cluster is located at the center of the cone base on the surface of the sphere. The base radius in the single-channel case is 1.5 μm and in the cluster case is 3.3 μm. *B*, *top*: submembrane Ca^{2+} concentrations (color coded; in μM) as a function of time and the distance to the channel (d; measured along the cone base as indicated in *A*) during spiking electrical activity. *B*, *bottom*: Ca^{2+} concentration at 500 nm from the channel as function of time.

whereas others exhibit voltage-dependent inactivation. We found that fixed-rate constants $k_- = 0.018\ ms^{-1}$ and $k_+ = 0.0324\ ms^{-1}$ were sufficient to match inactivation experimentally observed by Hagiwara and Ohmori (11). The stochastic channel dynamics (*Eq. 3*) were simulated as realizations of the discrete-state, continuous-time Markov chain, with transition probabilities for a small time step Δt described by

$$\begin{bmatrix} O(t+\Delta t) \\ C(t+\Delta t) \\ B(t+\Delta t) \end{bmatrix} = \begin{bmatrix} 1-(\beta+k_+)\Delta t & \alpha\Delta t & k_-\Delta t \\ \beta\Delta t & 1-\alpha\Delta t & 0 \\ k_+\Delta t & 0 & 1-k_-\Delta t \end{bmatrix} \begin{bmatrix} O(t) \\ C(t) \\ B(t) \end{bmatrix}. \quad (5)$$

Monte Carlo simulations were performed, and the single-channel open state $O(t)$ was used to compute the single-channel current as

$$I_{sc}(t) = g_{sc}O(t)(V(t) - V_{Ca}) \quad (6)$$

where g_{sc} is the single-channel conductance. In the cluster case, the total current is simulated by summing five independent realizations of a single-channel current (I_{sc}). Both the current driving force and open probability are coupled to the time-varying membrane potential $V(t)$. Specifically, the driving force decreases as $V(t)$ increases toward the Ca^{2+} reversal potential V_{Ca}, whereas the open probability increases with $V(t)$.

Endogenous buffers. In all simulations we assumed the presence of a single immobile endogenous Ca^{2+} buffer, in agreement with Kits et al. (15), and no mobile buffers were considered. Binding of Ca^{2+} to the buffers is described by simple mass action kinetics with one-to-one stoichiometry,

$$B + Ca^{2+} \underset{k_{off}}{\overset{k_{on}}{\rightleftarrows}} CaB, \quad (7)$$

where k_{on} and k_{off} are association and disassociation rates, respectively. The reaction-diffusion equations for the Ca^{2+} concentration and the free unbound buffers are taken from (20)

$$\frac{\partial[Ca^{2+}]}{\partial t} = D_{Ca}\nabla^2[Ca^{2+}] - k_{on}[Ca^{2+}][B] + k_{off}(B_{total} - [B]) + \frac{1}{2F}I_{sc}(t)\delta(r - R, \theta) - k_{uptake}([Ca^{2+}] - [Ca^{2+}]_0), \quad (8)$$

$$\frac{\partial[B]}{\partial t} = -k_{on}[Ca^{2+}][B] + k_{off}(B_{total} - [B]), \quad (9)$$

where D_{Ca} is the diffusion coefficient for unbound Ca^{2+}. We chose $D_{Ca} = 0.2\ \mu m^2/ms^{-1}$ (1) and assumed that the distribution of the immobile buffer is spatially uniform. The second-to-last term in *Eq. 8* represents Ca^{2+} influx, where F is Faraday's constant, $I_{sc}(t)$ is the (inward) single-channel (or 5-channel cluster) calcium current, and $\delta(r - R,\theta)$ is the Dirac δ-function centered at $r = R$ and $\theta = 0$ (i.e., at the center of the base of the cone). The last term defines net Ca^{2+} uptake into internal stores such as the endoplasmic reticulum with constant rate $k_{uptake} = 0.3$ μM/ms. $[Ca^{2+}]_0$ is the Ca^{2+} concentration in case of no Ca^{2+} influx and spatiotemporal equilibrium. In accordance with simulation studies performed by Kits et al. (15) in melanotroph cells, we set the endogenous buffer parameters $k_{on} = 0.1\ \mu M^{-1}ms^{-1}$, $K_D = k_{off}/k_{on} = 10$ μM, and $B_{total} = 900$ μM. No-flux boundary conditions hold for Ca^{2+} at all boundaries. The reaction-diffusion equations were solved using the Calcium Calculator (CalC) software developed by Matveev (21). CalC uses an alternating-direction implicit finite difference method with second-order accuracy in space and time and with adaptive time steps.

Exocytosis model. We initially used a six-pool exocytosis model (4), which describes the fraction of granules in various pools of granules described as docked, primed, domain bound, or in one of three prefusion states distinguished by the number of bound Ca^{2+} ions. However, for the relatively short time courses used here (5 s), our preliminary simulations showed no significant differences between this six-pool model and a simpler four-pool model in which the docked, primed, and domain-bound pools were combined into a single pool that we call the "primed" pool. We use this simplified model (Fig. 2), which is similar to a model of exocytosis in melanotroph cells (15) in all simulations. Here, the granule can be in one of four different states: a primed state where the granule is adjacent to the plasma membrane (N_0), or states in which one (N_1), two (N_2), or three (N_3) Ca^{2+} ions are bound to the Ca^{2+} sensor, likely synaptotagmin (31). Once in state N_3, the granule fuses with the membrane and releases its hormone content at rate u_1. Granule release is triggered by local Ca^{2+} levels (C_{loc}), as indicated in Fig. 2, whereas resupply is dependent on the bulk calcium concentration C_i, which is computed as the submembrane Ca^{2+} concentration 1.5 μm from the channel. The rate of resupply per cell r_1 is

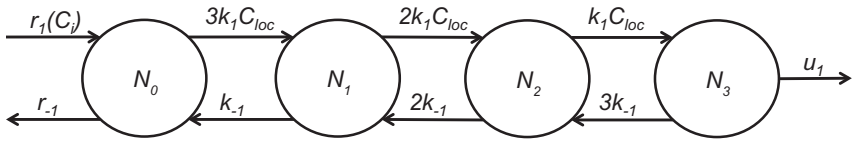

Fig. 2. Kinetic scheme of the exocytosis model. The pool N_0 consists of granules primed for fusion, and its resupply depends on the bulk cytosolic Ca^{2+} concentration C_i. Fusion occurs upon Ca^{2+} binding controlled by the local concentration of Ca^{2+}, C_{loc}. The pools N_1, N_2, and N_3 correspond to the 3 Ca^{2+}-bound states, and u_1 is the fusion rate.

$$r_1 = \frac{C_i(t) r_1^0}{C_i(t) + K_p}, \tag{10}$$

where $K_p = 2.3$ μM (4, 40) and $r_1{}^0$ is the maximal resupply rate per cell.

All secretion model steps are assumed to be reversible, except for fusion. The local Ca^{2+} concentration was determined by solving the Ca^{2+} reaction-diffusion equations and using the Ca^{2+} value at the release site (*Eqs. 8* and *9*). The exocytosis model describing release per cell is given by the following differential equations:

$$\begin{aligned}
\frac{dN_0}{dt} &= -\left(3k_1 C_{loc}(t) + r_{-1}\right)N_0 + r_1\left(C_i(t)\right) + k_{-1}N_1,\\
\frac{dN_1}{dt} &= -\left(2k_1 C_{loc}(t) + k_{-1}\right)N_1 + 3k_1 C_{loc}(t)N_0 + 2k_{-1}N_2,\\
\frac{dN_2}{dt} &= -\left(k_1 C_{loc}(t) + 2k_{-1}\right)N_2 + 2k_1 C_{loc}(t)N_1 + 3k_{-1}N_3,\\
\frac{dN_3}{dt} &= -\left(u_1 + 3k_{-1}\right)N_3 + k_1 C_{loc}(t)N_2,
\end{aligned} \tag{11}$$

where N_i is the number of granules in pool i. Experimental data (37) indicate a relatively low Ca^{2+} binding affinity; as a consequence, we use the Ca^{2+} affinity value $k_d = k_{-1}/k_1 = 27$ μM in *Eq. 11*.

We used two sets of initial conditions for the granule/exocytosis model. In the model of Chen et al. (4), the number of primed granules (pool N_0) is equal to 40 per cell. Hence, we set as the initial condition $N_0 = 40$ primed granules, each a fixed distance from a single channel (so that 35 channels are not associated with granules). Assuming that, in any one simulation, all Ca^{2+} channels in the cell behave identically according to the Markov simulation, the granules will be exposed to the same Ca^{2+} profile. To calculate average cellular exocytosis, we performed 10 (single channel) or five (cluster) simulations and computed average values of N_i at each time point.

This initial condition ($N_0 = 40$) reflects experiments such as single-cell capacitance measurements of triggered exocytosis, where no exocytosis is occurring before the experiment (36, 37). For interpreting hormone secretion experiments, where secretion is ongoing, the steady state of the model is more relevant. We found that the pools empty within seconds (see RESULTS), and therefore, we considered initial conditions where all pools are empty to reflect secretion experiments.

The exocytosis rate per cell, with N_3 the average of 10 or five trials, as explained above, is

$$J_F(t) = u_1 N_3(t), \tag{12}$$

and the cumulative number of fused granules per cell is

$$M_F(t) = \int_0^t u_1 N_3(t')dt'. \tag{13}$$

To show how much of the simulated secretion is due to increased Ca^{2+} influx during bursting compared with spiking electrical activity, that is, to investigate whether bursting increases the Ca^{2+} current sensitivity of exocytosis (26), we related exocytosis to the total charge entering via the Ca^{2+} channel or channel cluster (26):

$$Q(t) = \int_0^t I_{sc} ds. \tag{14}$$

The exocytosis model was solved using the MATLAB (R2012b; The MathWorks) function ode15s.

RESULTS

Secretion Evoked By Ca^{2+} Influx Through Single Channels is Increased When Converting Spiking to Bursting Electrical Activity Through Dynamic Clamp

Gonadotrophs release little LH under basal conditions, which has been suggested to be associated with their typical spiking electrical behavior (10). We have previously shown that adding a BK-type K^+ current to a spiking gonadotroph can change its behavior into bursting (35). Figure 3 shows an example of such a cell where the injected BK-type current induces bursting in an otherwise spiking gonadotroph. We also show the average of 10 independent simulations, each with a stochastic Ca^{2+} channel providing Ca^{2+} to the interior of the cell and subsequent Ca^{2+} diffusion. The Ca^{2+} model is driven by either the spiking voltage pattern (Fig. 3*A*) or the bursting pattern (Fig. 3*B*) obtained by injecting a BK-type K^+ current via dynamic clamp. Average Ca^{2+} profiles are reported at distances of 30, 200, and 1,500 nm from the Ca^{2+} channel. As expected, close to the channel, i.e., 30 nm, Ca^{2+} reaches high concentrations of some tens of micromolar on average with peaks up to ~70 μM during spiking activity and ~110 μM during bursting. The traces are very noisy due to the stochastic openings of the Ca^{2+} channel. The average Ca^{2+} concentration decreases with distance from the channel, reaching <1 μM at a distance of 1,500 nm. In addition, the noise is attenuated due to the effects of diffusion, which acts as a low-pass filter. Ca^{2+} measurements using a fluorescent dye such as fura-2 report on the Ca^{2+} concentration averaged over the cell and have time courses similar to those shown in the bottom row of Fig. 3 (30, 32).

We now locate the exocytosis machinery at different distances from the Ca^{2+} channel and use the Ca^{2+} concentration at that location to drive the exocytosis model (Fig. 2 and *Eq. 11*). Figure 4 shows the average number of fused granules over time at different distances. If the release site is 30 nm from the channel, it is exposed to very high Ca^{2+} concentrations whether the cell is spiking or bursting, and exocytosis occurs at its maximum rate that releases all of the granules in the primed pool N_0 (40 granules) very soon after the start of the input train. A similar result occurs if the release site is located 100 nm from the channel. Thus, if the release site and channel are within 100 nm of each other, it does not matter whether the cell is spiking or bursting; the secretion level will be the same since the Ca^{2+} concentrations at the exocytotic machinery are in

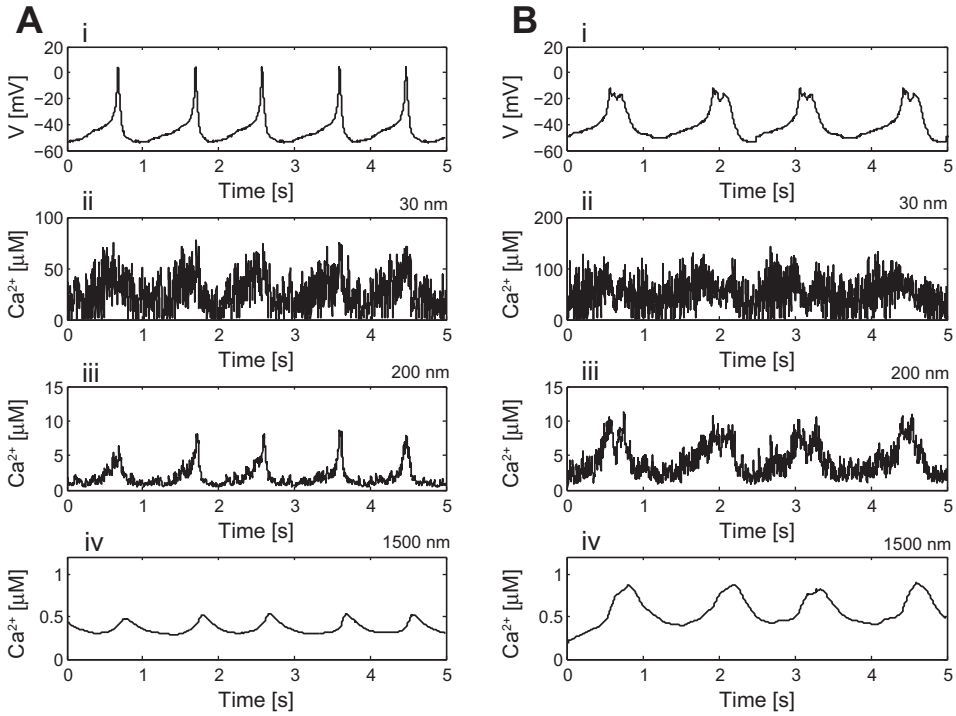

Fig. 3. Ca^{2+} concentration at different distances from a single stochastic Ca^{2+} channel on the surface of a conical region (average of 10 independent trials). The Ca^{2+} channel is placed at the center of the cone base with a radius of 1.5 μm. The Ca^{2+} concentration is determined using a mathematical model in response to actual spiking (*A*) and bursting (*B*) voltage traces from a gonadotroph. The switch to bursting was obtained by injecting a model large-conductance potassium (BK) current into a spiking cell using the dynamic clamp technique.

both cases saturating. At a distance of 200 nm, there is a difference between exocytosis evoked by spiking and that evoked by bursting; the bursting pattern (solid) evokes release at a higher rate than the spiking pattern (dashed), although both release almost all available granules by the end of the 5-s input train. The advantage of bursting over spiking is amplified when the release site is situated further from the channel, at 300 or 500 nm. Although the absolute number of fused granules is lower when the channel and the release site are more distant, the bursting voltage trace releases more granules than the spiking trace at all time points. Thus, our simulations support the notion that adding an outward K^+ current can, by changing spiking to bursting activity, increase secretion (6, 29).

These observations imply that the primed pool of granules can be emptied very quickly, and this fusion process is likely monitored with capacitance measurements of exocytosis that take place over a short period of time (14). In our data, the spiking voltage trace shows five spikes in 5 s, with each spike lasting ~40 ms (Fig. 3*A*, *i*). On average, each 40-ms depolarization of a pulse train was found to evoke ~10 fF of exocytosis (19). Thus, based on these experiments, we expect ~50 fF exocytosis during the 5 s shown in Fig. 3. In our simulations, exocytosis at a distance of 200 nm from the channel is ~30 granules. If we assume that a single granule corresponds to ~2 fF (39, 42), we get a capacitance measurement of ~60 fF, which is close to the ~50 fF calculated from the data in Ref. 19.

However, most secretion measurements are made from a cell population over a period of minutes or tens of minutes. In such measurements the resupply of the primed pool by the reserve granule pool is rate limiting. We next look at the effects of resupply by emptying the primed pool N_0 at the beginning of the simulation and from this initial condition evaluate the differential exocytosis evoked by spiking and bursting.

The cumulative number of fused granules as a function of time is shown in Fig. 5, *top*. Bursting evokes more release regardless of the distance between the channel and the granule. This is despite the fact that at short distances the local Ca^{2+} concentration saturates the release site and highlights the importance of the dependence of resupply on the global, rather

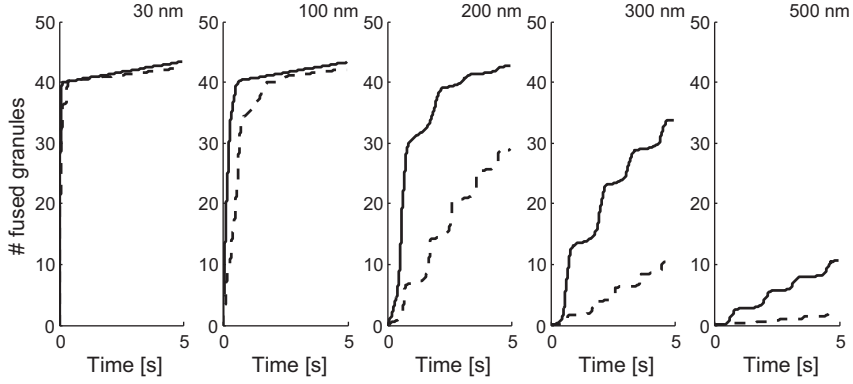

Fig. 4. Single-channel exocytosis simulation results with $N_0 = 40$ primed granules as initial condition. No. of fused granules (average of 10 simulations) during spiking (dashed curved line) and bursting (solid curved line) electrical activity for different distances between the single Ca^{2+} channel and a release site as a function of time.

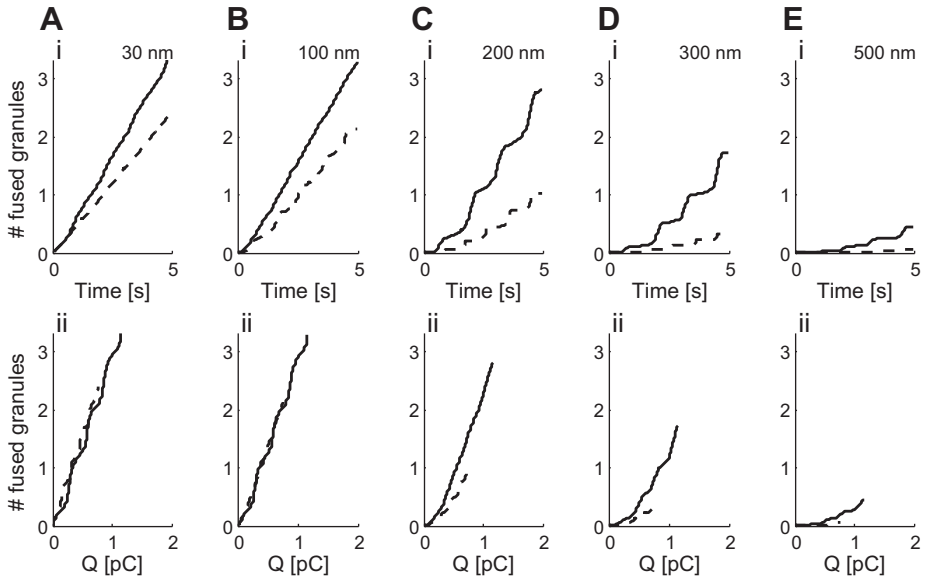

Fig. 5. Single-channel exocytosis simulation results with all of the pools initially empty. *Top* (*i*): no. of fused granules as a function of time, as in Fig. 4. *Bottom* (*ii*): cumulative no. of fused granules during 5 s of simulation as function of the cumulative calcium entry Q. Granules located at 30 (*A*), 100 (*B*), 200 (*C*), 300 (*D*), or 500 nm (*E*) from the channel.

than local, Ca^{2+} concentration. That is, the simulated global Ca^{2+} concentration is higher during bursting than during spiking, as measured by fluorescent dyes (22), and this results in a greater rate of resupply in response to bursting. When the channel is close to the release site, all granules becoming available due to the resupply are fused almost immediately, so resupply is rate limiting. Farther than 200 nm from the channel, local Ca^{2+} concentrations start to play a predominant role since the exocytosis machinery is no longer saturated, and therefore, differences in local Ca^{2+} levels as well as global levels are responsible for differences in the exocytosis rates.

There are two factors that could contribute to the greater effectiveness of bursting at evoking secretion in the model. One is that bursting brings in more Ca^{2+} over the 5 s of simulation time, increasing resupply rate relative to spiking, as mentioned above. The other is that the dynamics of Ca^{2+} diffusion and the exocytotic machinery favor the bursting signal over the spiking signal. That is, bursting is more efficient than spiking at evoking release. To test the latter, we plot the number of fused granules vs. the total Ca^{2+} entry Q (Fig. 5, *bottom*). For release sites closer than 200 nm from the channel, the efficiencies of the spiking and bursting patterns are virtually the same. It is only at distances of $\geq$200 nm that bursting becomes more efficient than spiking, since at these distances the number of fused granules per total Ca^{2+} entry is larger when the cell is bursting. This is due to the longer duration of the bursting events, which produce longer-duration Ca^{2+} signals that are advantageous for the exocytosis machinery that requires the binding of three Ca^{2+} ions to evoke granule fusion. In fact, in simulations in which only two Ca^{2+} ions are needed to evoke fusion, the efficiencies of spiking and bursting are the same at a 200-nm distance, and bursting is only slightly more efficient at 300- and 500-nm distances (not shown).

As a final quantification of the effectiveness of bursting vs. spiking at evoking secretion, we show the ratio between bursting-evoked secretion and spiking-evoked secretion in Fig. 6, solid line. This ratio is calculated from the total number of fused granules at the end of the 5-s input voltage train as a function of distance between the channel and the release site. Up until a distance of 100 nm, the ratio is ~1.5; the burst pattern evokes a slightly higher amount of secretion than spiking. Past this distance the ratio increases continuously, reaching a value of ~8.5 at a distance of 700 nm. Thus, there is between 1.5 and 8.5 times more secretion by the end of the 5-s stimulation with bursting vs. spiking. Plotting the ratio of exocytosis during spiking and bursting but normalized to the charge Q (Fig. 6, dashed line) shows that spiking and bursting have almost the same Ca^{2+} current sensitivity close to the channel (i.e., they are equally efficient at evoking release), but farther away bursting becomes more efficient than spiking,

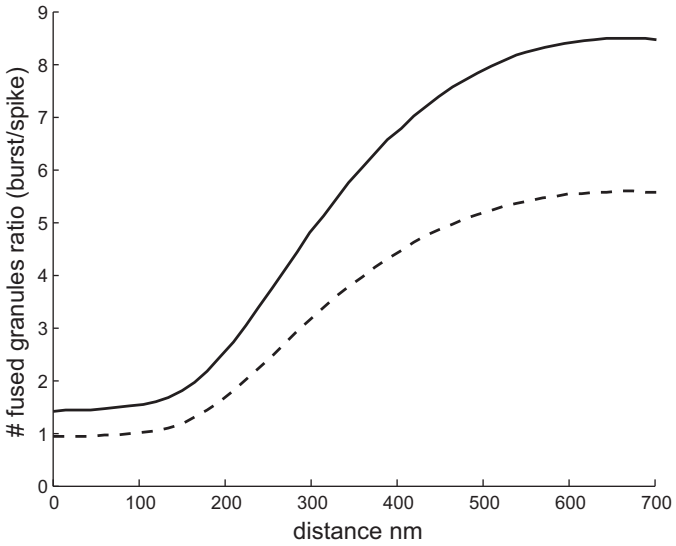

Fig. 6. Summary of single-channel exocytosis results with all of the pools initially empty. The bursting-to-spiking ratio of the total no. of fused granules during 5 s of electrical activity (solid line) shows that bursting evokes more secretion at all distances. In contrast, the bursting-to-spiking ratio of the total no. of granules normalized to change entry Q (dashed line) shows that the efficiencies of spiking and bursting are comparable for release sites located close to the channel but that bursting has superior efficiency farther from the channel.

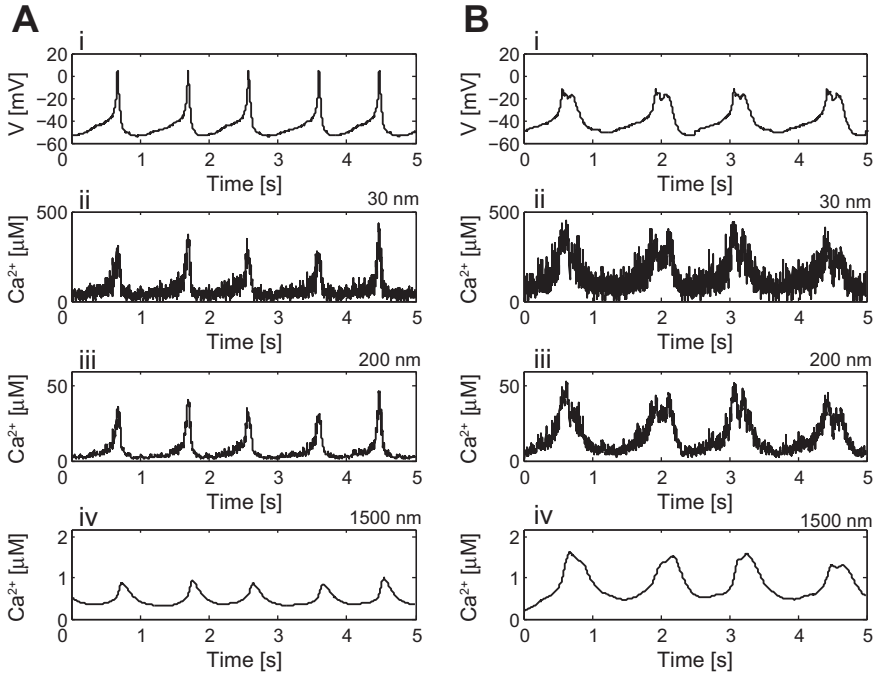

Fig. 7. Ca^{2+} concentrations for a cluster of 5 channels (average of 5 independent trials). The Ca^{2+} channel is placed at the center of the cone base with a radius of 3.3 μm. The Ca^{2+} concentration is determined using the mathematical model in response to actual spiking (*A*) and dynamic clamp-induced bursting (*B*) voltage traces from a gonadotroph (same traces as in Fig. 3).

reaching a 5.5-fold higher Ca^{2+} current sensitivity at a distance of 700 nm from the channel.

In summary, our simulations suggest that LH secretion from a gonadotroph could increase substantially if the electrical pattern switched from spiking to bursting, for example, because of the addition of a BK-type current.

Secretion Evoked By Ca^{2+} Influx Through a Cluster of Channels

The previous simulations assumed that each release site is acted upon by Ca^{2+} from single channels, and indeed there is evidence supporting this, in both endocrine cells and neuronal synapses (11, 17). However, it is likely that hormone release sites receive Ca^{2+} from several channels, and there is also evidence for this (2, 3). In the next set of simulations, we consider such a situation where a release site is affected by Ca^{2+} from a cluster of five stochastic Ca^{2+} channels. For simplicity, we assume that these are equidistant from the release site.

Figure 7 shows the Ca^{2+} concentration at different distances from the channel cluster in response to the spiking or bursting voltage trace. Close to the cluster (30 nm), Ca^{2+} rises to a level of several hundreds of micromolar, about five times larger than in the single-channel case. At greater distances, the increase over the single-channel level is less, since now the different clusters are 6,600 nm apart so that a release site located 1,500 nm from a cluster is >5,000 nm from the next nearest cluster. In contrast, with uniform distribution of the same number of channels (the single channel case), a release site located 1,500 nm from one channel was located the same distance from a second channel, so it received an equal amount of Ca^{2+} from both. Hence, whereas a cluster of five channels provides approximately five times higher Ca^{2+} levels to granules located close to the channels, a granule located 1,500 nm from channels will be exposed to just $\sim 5/2 = 2.5$ times higher Ca^{2+} concentrations in the case of channel clusters compared with the single-channel configuration.

Figure 8, *top*, shows that bursting is always superior to spiking in evoking exocytosis when channels are in clusters and the primed pool is initially empty. In contrast, the difference in Ca^{2+} current sensitivity is hardly observable when the release site is <300 nm from the channel cluster (Fig. 8, *bottom*). Therefore, it is mostly the larger amount of Ca^{2+} entering during bursting that determines the difference in secretion. Figure 9 summarizes the results for channel clusters. Even at the closest release site/cluster distances, the bursting-to-spiking ratio of the total number of fused granules is ~1.5 and increases to ~4.5 at 700 nm (Fig. 9, solid line). The relative efficiency, i.e., the bursting-to-spiking ratio of the total number of granules normalized to Ca^{2+} entry, is ~1 up to 300 nm and then increases to ~2.5 at 700 nm. Thus, just as with single-channel-evoked release, bursting provides more secretion than does spiking when exocytosis is triggered by channel clusters. However, the advantage of bursting over spiking becomes manifest at greater distances for clusters than for single channels, 100 nm in Fig. 6 vs. 300 nm in Fig. 9. Because the trends are qualitatively similar with single-channel and cluster-evoked secretion, we focus on only one type (single-channel secretion) in the remaining simulations.

Bursting Superiority Depends on the Frequency of Spiking

As a second example, we now use recordings from a GH4 cell line. It has been shown previously that pseudo-plateau bursting in some pituitary cells converts to spiking when BK-type K^+ channels are pharmacologically blocked, reducing the bulk Ca^{2+} concentration (8). Does this manipulation also result in a decrease in the domain Ca^{2+} and, therefore, in decreased secretion? We have shown that bursting can be rescued by adding BK current back to the cell using the dynamic clamp technique (here and in Ref. 34). In Fig. 10, we

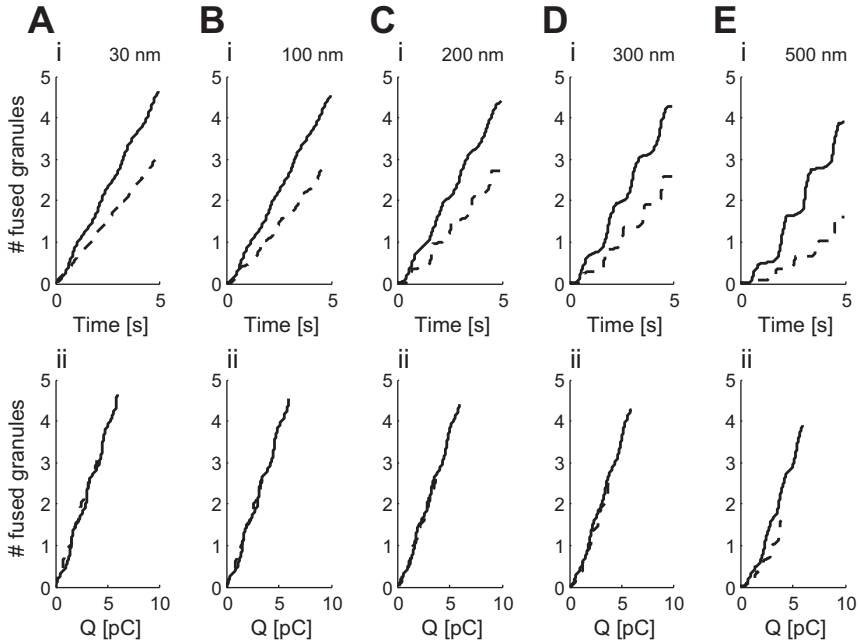

Fig. 8. Channel cluster exocytosis simulation results with all of the pools initially empty. *Top* (*i*): no. of fused granules as a function of time evoked by spiking (dashed curved line) or bursting (solid curved line). *Bottom* (*ii*): cumulative no. of fused granules during 5 s of simulation as a function of the cumulative Ca^{2+} entry Q. Granules located at 30 (*A*), 100 (*B*), 200 (*C*), 300 (*D*), or 500 nm (*E*) from the channel.

use both procedures. We begin with a bursting lacto-somatroph GH4C1 cell (Fig. 10*A*) and then convert it to a spiking cell by the addition of the BK channel blocker iberiotoxin (Fig. 10*B*), and then finally we convert the spiking cell back to a bursting cell using dynamic clamp to inject a model BK current (Fig. 10*C*). For each case, we calculate the Ca^{2+} concentration at varying distances from the single stochastic channel, as in prior simulations. Close to the channel, the Ca^{2+} concentration is about the same for all three voltage traces. However, at the greater distances, e.g., 1,500 nm, the Ca^{2+} levels corresponding to the bursting voltage traces are higher than those corresponding to the spiking voltage trace, as has been observed in experiments (18).

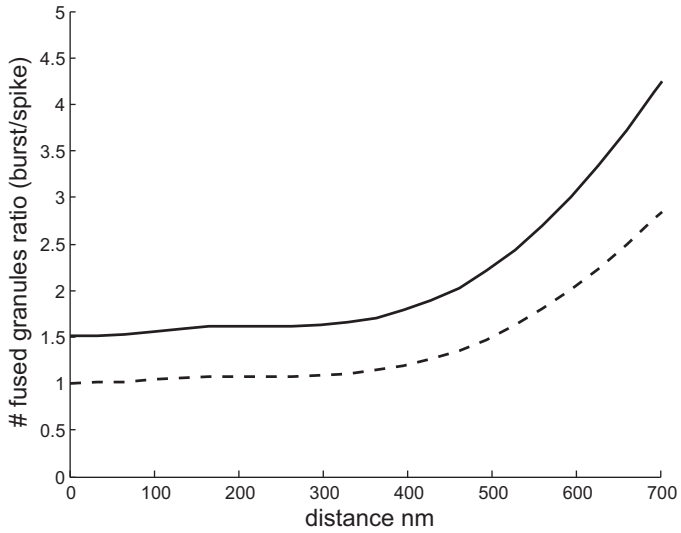

Fig. 9. Summary of channel cluster exocytosis results with all of the pools initially empty. The bursting-to-spiking ratio of the total no. of fused granules during 5 s of electrical activity (solid line) shows that bursting evokes more secretion at all distances. In contrast, the bursting-to-spiking ratio of the total no. of granules normalized to change entry Q (dashed line) shows that the efficiencies of spiking and bursting are comparable for release sites located close to the channel cluster but that bursting has superior efficiency farther away.

We next use these Ca^{2+} time courses to simulate exocytosis for release sites located at different distances from the Ca^{2+} channel (Fig. 11). The results are summarized in Fig. 12, where we show the number of fused granules evoked by the dynamic clamp-induced bursting vs. that evoked by the spiking trace (Fig. 11, solid black curved line). In both cases, the ratio is near 1 up until a separation distance of ~150–200 nm. At greater separations the ratio increases, indicating that at these greater distances the bursting trace is more effective at evoking exocytosis than the spiking trace. Normalizing to Ca^{2+} influx reveals that the ratio of Ca^{2+} current sensitivity is higher for spiking close to the channel (ratio <1), whereas bursting is more efficient farther from the channel (Fig. 12). The fact that bursting is less superior to spiking after normalizing to Ca^{2+} influx compared with the previous simulations of exocytosis using the traces from a gonadotroph (Figs. 5 and 6) can be explained by noticing that, for this example, iberiotoxin-induced spiking (Fig. 10*B*) occurs at a much higher rate (~1.8 Hz) than bursting (~0.8 Hz; Fig. 10, *A* and *C*). Thus, the dynamics of Ca^{2+} entry are important for the control of exocytosis in addition to the number of Ca^{2+} ions entering the cell.

DISCUSSION

In the absence of hypothalamic stimulation or inhibition, pituitary lactotrophs and somatotrophs release prolactin and growth hormone, whereas gonadotrophs comparatively secrete a negligible amount of luteinizing hormone. This difference in basal hormone release was matched by differences in spontaneous electrical activity between these cell types; lactotrophs and somatotrophs often exhibit "pseudo-plateau" bursts of activity, causing periodic Ca^{2+} influx, whereas gonadotrophs usually produce spikes that are too brief to perturb the bulk

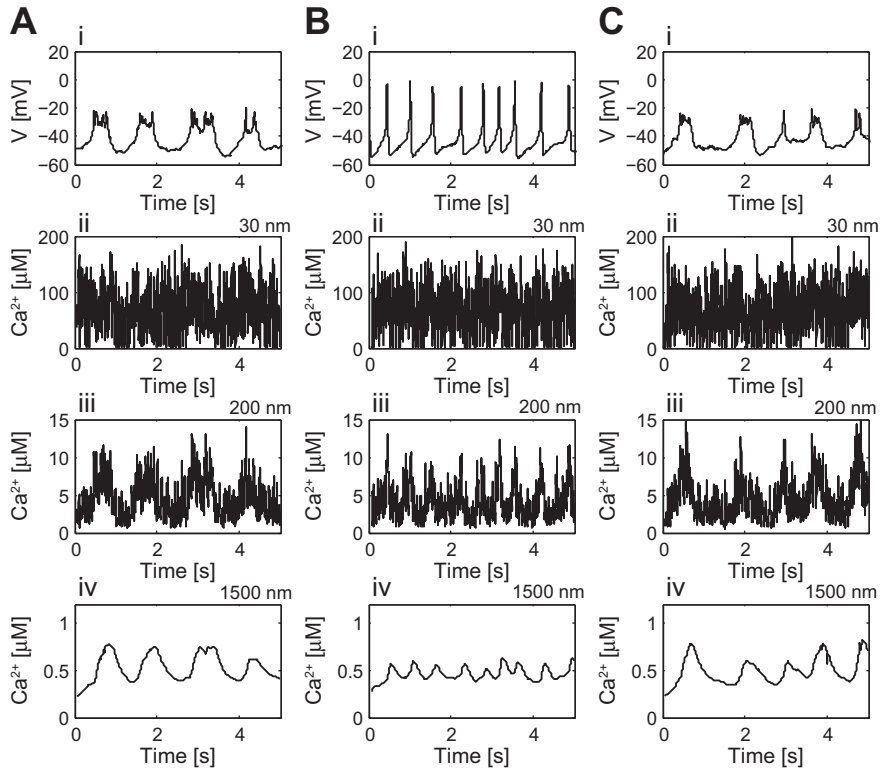

Fig. 10. Ca^{2+} concentration at different distances from a stochastic Ca^{2+} channel on the surface of a conical region (average of 10 independent trials). The Ca^{2+} channel is placed at the center of the cone base with radius of 1.5 μm. *A*: bursting profile in control condition. *B*: spiking profile in the presence of the BK channel blocker iberiotoxin. *C*: bursting profile in the presence of iberiotoxin and when BK current is injected back using the dynamic clamp. Graphs show the experimentally recorded voltage profile (*i*) and simulated Ca^{2+} concentrations at 30 (*ii*), 200 (*iii*), or 1,500 nm (*iv*) from the channel.

Ca^{2+} level substantially (9). Such differences in the bulk Ca^{2+} profiles lead to the hypothesis that different patterns of spontaneous electrical activity result in different rates of hormone release. Bursting causes hormone release from lactotrophs and somatotrophs, whereas spiking causes no hormone release from gonadotrophs.

We tested this hypothesis in this study. Although Ca^{2+} triggers hormone release and bursting creates larger amplitude oscillations of average intracellular Ca^{2+} than spiking, this does not necessarily mean that bursting is more effective at triggering hormone release. The Ca^{2+} concentration that matters is that seen by the hormone-containing granules at their release sites, and if the release sites are close to Ca^{2+} channels, the high Ca^{2+} concentration in the microdomains around the channels created by a single spike may be just as effective as that due to a burst in triggering fusion of granules. Indeed, we found that

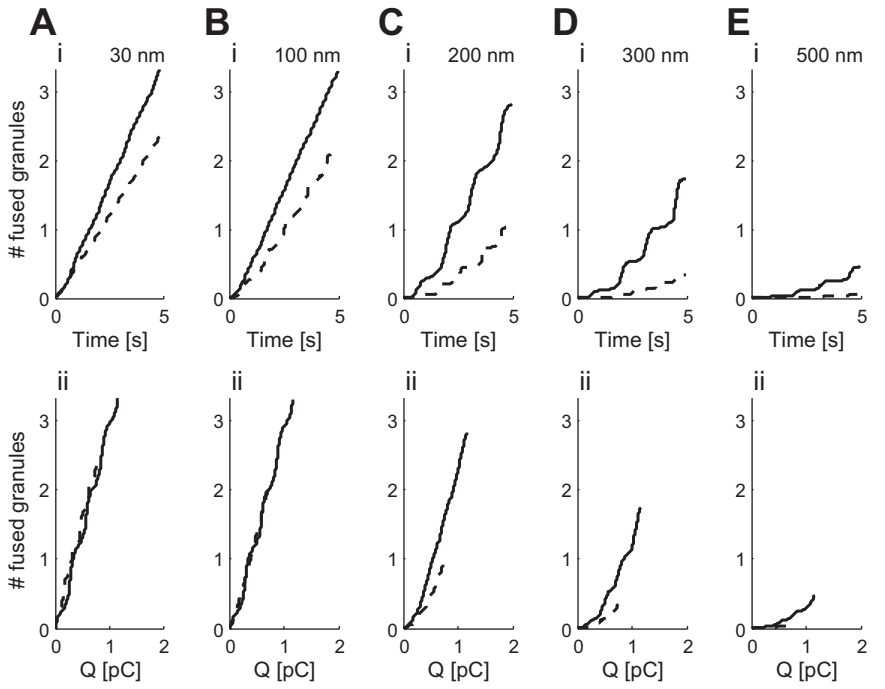

Fig. 11. Single channel exocytosis simulation results with all of the pools initially empty for dynamic clamp-induced bursting. *Top* (*i*): no. of fused granules as a function of time evoked by a spiking voltage trace (dashed curved lines) and bursting induced by dynamic clamp in the presence of iberiotoxin (solid curved lines). *Bottom* (*ii*): cumulative no. of fused granules during 5 s of simulation as a function of the cumulative Ca^{2+} entry Q. Granules are located at 30 (*A*), 100 (*B*), 200 (*C*), 300 (*D*), or 500 nm (*E*) from the channel.

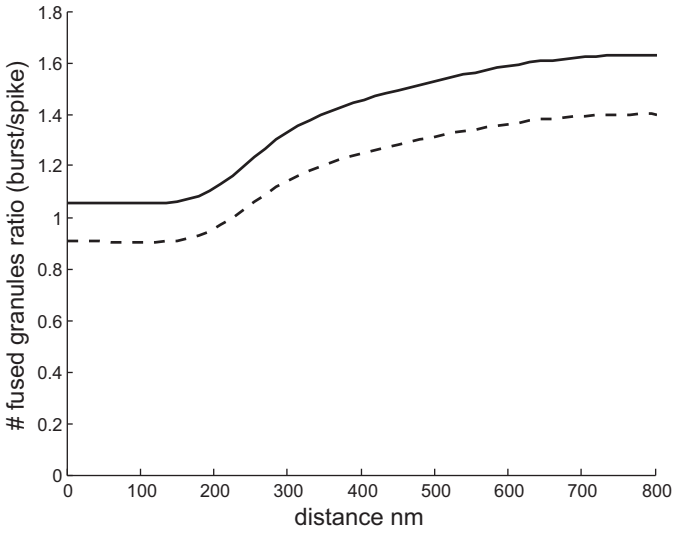

Fig. 12. Summary of exocytosis simulation results with all of the pools initially empty during BK current block and dynamic clamp. Ratios of the total no. of fused granules between bursting that results from dynamic clamp application with iberiotoxin vs. spiking that results from iberiotoxin alone (solid curved line). Ratios of the total no. of fused granules normalized to the charge entry Q are given by the dashed curved line.

spiking is as effective as bursting in releasing a full pool of primed granules, as long as the release site is within 100 nm from the channel (Fig. 4). However, if the primed pool of granules is initially empty, or if the release site is located more than 100 nm from the channel, we found that bursting was always more effective than spiking in triggering granule fusion.

There are two mechanisms for this difference between bursting and spiking. The first results from the larger entry of Ca^{2+} caused by bursting over spiking. Because the fraction of open Ca^{2+} channels is increased for a longer period of time during a burst than during a spike, a burst causes a larger increase in bulk Ca^{2+}. Since the replenishment of the primed pool of granules depends on bulk Ca^{2+}, bursting causes a higher rate of granule priming, which in turn results in a higher rate of granule fusion. This effect is independent of the microdomain Ca^{2+} concentration, so bursting causes a higher rate of granule fusions even if the release site is 100 nm or less from the channel (Fig. 5, *top*). However, this mechanism relies on the fact that, at similar event frequency, bursting means that the electric potential across the cell membrane stays high (i.e., at levels where the cell Ca^{2+} current is high) for a larger fraction of time than spiking. If spiking frequency is increased relative to bursting frequency so that the total amount of active time is the same, then bulk Ca^{2+} will be similar, and so will the priming rate. In that sense, the bursting pattern is not more effective than the spiking pattern if the amount of activity (and therefore, Ca^{2+} entry) is normalized.

Nevertheless, there is a second mechanism that makes bursting more effective than spiking at triggering granule fusion, even if we normalize by the total amount of Ca^{2+} entry. Because three free Ca^{2+} ions must bind to the release machinery to trigger fusion, fusion is facilitated by a stable high local Ca^{2+} level. This is more likely to happen during bursting than spiking, since Ca^{2+} influx can be maintained longer during a burst than during a spike. This advantage of bursting can be observed when the release site is more than 100 nm away from the channel (Fig. 5, *bottom*). Cells must quickly restore intracellular Ca^{2+} to low levels using ATP-driven pumps, so there is an energetic cost associated with the entry of each Ca^{2+} ion. For release sites far from the Ca^{2+} channels, the bursting pattern of activity results in a more efficient use of Ca^{2+} ions than the spiking pattern.

This may not be true at higher spike frequencies. If we increase spike frequency, the interval between each increase in local Ca^{2+} goes down, so the higher effectiveness of bursting might be observed only for release sites further away from the channels. We see that for the BK (endogenous or injected by dynamic clamp) vs. no BK case (i.e., in the presense of iberiotoxin), the maximum Ca^{2+} concentration at 200 nm (Fig. 10) is similar to what we found in Fig. 3. However, the interspike interval is shorter so that Ca^{2+} does not go back down for long, and therefore, spiking is at least as efficient as bursting in evoking secretion for release sites up to 500 nm away from the channels (Fig. 11). Nevertheless, the bursting pattern caused by the presence of a BK current evoked more granule fusion because of the high average bulk Ca^{2+} during bursting, which results in higher rate of replenishment of the primed granules.

There are many examples in endocrinology where the pattern of a signal plays an important role. A well-known example is that the frequency of hypothalamic gonadotropin-releasing hormone pulses determines the differential release of luteinizing and follicle-stimulating hormone by gonadotrophs (41). Here, we used a hybrid experimental/modeling approach to show that the actual pattern of electrical activity can trigger different rates of hormone release. Ever since the discovery 40 years ago that pituitary cells are electrically active, researchers have wondered how pituitary cells tune electrical activity to regulate hormone release (24). It has been argued that since hypothalamic factors act on a number of ion channels on pituitary cell membranes, electrical activity provides numerous ways for the hypothalamus to modulate pituitary hormone release. Some of these factors may even modulate the time constant of BK channels to switch the electrical activity pattern from spiking to bursting (6). The present work shows that this switch to bursting may improve the effect of hypothalamic stimulating neurohormones in increasing pituitary hormone secretion.

In summary, our modeling results show that bursting is superior to spiking in evoking pituitary hormone release, since it brings more Ca^{2+} into the cell, thus augmenting both local and global Ca^{2+} levels, which in turn increases resupply of secretory granules and exocytosis. Additionally, we found that channel clustering is advantageous to isolated channels in controlling secretion. Our results have implications beyond pituitary secretion. For example, human pancreatic β-cells show rapid bursting resembling pituitary plateau bursting (23, 27), which has been suggested to be advantageous for insulin secretion (25). Furthermore, Ca^{2+} channel clustering in β-cells has been suggested to be important for insulin exocytosis (2).

GRANTS

J. Tabak and R. Bertram were partially supported by Grant No. DMS1220063 from the National Science Foundation.

DISCLOSURES

No conflicts of interest, financial or otherwise, are declared by the authors.

AUTHOR CONTRIBUTIONS

A.T. and J.T. performed experiments; A.T. and M.G.P. analyzed data; A.T., J.T., R.B., and M.G.P. interpreted results of experiments; A.T. prepared figures; A.T., J.T., R.B., and M.G.P. drafted manuscript; A.T., J.T., R.B., and M.G.P. edited and revised manuscript; A.T., J.T., R.B., and M.G.P. approved final version of manuscript; R.B. and M.G.P. conception and design of research.

REFERENCES

1. **Allbritton NL, Meyer T, Stryer L.** Range of messenger action of calcium ion and inositol 1,4,5-trisphosphate. *Science* 258: 1812–1815, 1992.
2. **Barg S, Ma X, Eliasson L, Galvanovskis J, Göpel SO, Obermüller S, Platzer J, Renström E, Trus M, Atlas D, Striessnig J, Rorsman P.** Fast exocytosis with few Ca(2+) channels in insulin-secreting mouse pancreatic B cells. *Biophys J* 81: 3308–3323, 2001.
3. **Bertram R, Smith GD, Sherman A.** Modeling study of the effects of overlapping Ca2+ microdomains on neurotransmitter release. *Biophys J* 76: 735–750, 1999.
4. **Chen Y, Wang S, Sherman A.** Identifying the targets of the amplifying pathway for insulin secretion in pancreatic beta-cells by kinetic modeling of granule exocytosis. *Biophys J* 95: 2226–2241, 2008.
5. **Dubinsky JM, Oxford GS.** Ionic currents in two strains of rat anterior pituitary tumor cells. *J Gen Physiol* 83: 309–339, 1984.
6. **Duncan PJ, Sengul S, Tabak J, Ruth P, Bertram R, Shipston MJ.** Large conductance Ca(2+) -activated K(+) channels (BK) promote secretagogue-induced transition from spiking to bursting in murine anterior pituitary corticotrophs. *J Physiol* 593: 1197–1211, 2015.
7. **Freeman ME, Kanyicska B, Lerant A, Gyorgy N.** Prolactin: structure, function, and regulation of secretion. *Physiol Rev* 80: 1523–1631, 2000.
8. **Van Goor F, Li YX, Stojilkovic SS.** Paradoxical role of large-conductance calcium-activated K+ (BK) channels in controlling action potential-driven Ca2+ entry in anterior pituitary cells. *J Neurosci* 21: 5902–5915, 2001.
9. **Van Goor F, Zivadinovic D, Martinez-Fuentes AJ, Stojilkovic SS.** Dependence of pituitary hormone secretion on the pattern of spontaneus voltage-gated calcium influx. Cell type-specific action potential secretion coupling. *J Biol Chem* 276: 33840–33846, 2001.
10. **Van Goor F, Zivadinovic D, Stojilkovic SS.** Differential expression of ionic channels in rat anterior pituitary cells. *Mol Endocrinol* 15: 1222–1236, 2001.
11. **Hagiwara S, Ohmori H.** Studies of single calcium channel currents in rat clonal pituitary cells. *J Physiol* 336: 649–661, 1983.
12. **Hodgking AL, Huxley AF.** A quantitative description of membrane current and its application to conduction and excitation in nerve. *J Physiol* 117: 500–544, 1952.
13. **Keja JA, Kits KS.** Single-channel properties of high- and low-voltage-activated calcium channels in rat pituitary melanotropic cells. *J Neurophysiol* 71: 840–855, 1994.
14. **Kits KS, Mansvelder HD.** Regulation of exocytosis in neuroendocrine cells: spatial organization of channels and vesicles, stimulus-secretion coupling, calcium buffers and modulation. *Brain Res Rev* 33: 78–94, 2000.
15. **Kits KS, de Vlieger TA, Kooi BW, Mansvelder HD.** Diffusion barriers limit the effect of mobile calcium buffers on exocytosis of large dense cored vesicles. *Biophys J* 76: 1693–1705, 1999.
17. **Klingauf J, Neher E.** Modeling buffered Ca2+ diffusion near the membrane: implications for secretion in neuroendocrine cells. *Biophys J* 72: 674–90, 1997.
18. **Li YX, Rinzel J, Vergara L, Stojilković SS.** Spontaneous electrical and calcium oscillations in unstimulated pituitary gonadotrophs. *Biophys J* 69: 785–795, 1995.
19. **Mansvelder HD, Kits KS.** The relation of exocytosis and rapid endocytosis to calcium entry evoked by short repetitive depolarizing pulses in rat melanotropic cells. *J Neurosci* 18: 81–92, 1998.
20. **Matveev V, Zucker RS, Sherman A.** Facilitation through buffer saturation: constraints on endogenous buffering properties. *Biophys J* 86: 2691–2709, 2004.
21. **Matveev V.** *CalC·The Calcium Calculator·Victor Matveev, NJIT* (Online). Homepage of Victor Matveev, Dept. of Mathematical Sciences, New Jersey Institute of Technology, Newark, NJ. https://web.njit.edu/~matveev/ [3 February 2016].
22. **Milescu LS, Yamanishi T, Ptak K, Mogri MZ, Smith JC.** Real-time kinetic modeling of voltage-gated ion channels using dynamic clamp. *Biophys J* 95: 66–87, 2008.
23. **Misler S, Barnett DW, Gillis KD, Pressel DM.** Electrophysiology of stimulus-secretion coupling in human beta-cells. *Diabetes* 41: 1221–1228, 1992.
24. **Mollard P, Schlegel W.** Why are endocrine pituitary cells excitable? *Trends Endocrinol Metab* 7: 361–365, 1996.
25. **Pedersen MG, Cortese G, Eliasson L.** Mathematical modeling and statistical analysis of calcium-regulated insulin granule exocytosis in beta-cells from mice and humans. *Prog Biophys Mol Biol* 107: 257–264, 2011.
26. **Pedersen MG.** On depolarization-evoked exocytosis as a function of calcium entry: possibilities and pitfalls. *Biophys J* 101: 793–802, 2011.
27. **Riz M, Braun M, Pedersen MG.** Mathematical modeling of heterogeneous electrophysiological responses in human β-cells. *PLoS Comput Biol* 10: e1003389, 2014.
28. **Sherman A, Keizer J, Rinzel J.** Domain model for Ca2(+)-inactivation of Ca2+ channels at low channel density. *Biophys J* 58: 985–995, 1990.
29. **Stojilkovic SS, Tabak J, Bertram R.** Ion channels and signaling in the pituitary gland. *Endocr Rev* 31: 845–915, 2010.
30. **Stojilkovic SS, Zemkova H, Van Goor F.** Biophysical basis of pituitary cell type-specific Ca2+ signaling-secretion coupling. *Trends Endocrinol Metab* 16: 152–159, 2005.
31. **Stojilkovic SS.** Ca2+-regulated exocytosis and SNARE function. *Trends Endocrinol Metab* 16: 81–83, 2005.
32. **Stojilkovic SS.** Pituitary cell type-specific electrical activity, calcium signaling and secretion. *Biol Res* 39: 403–423, 2006.
33. **Tabak J, Gonzalez-Iglesias AE, Toporikova N, Bertram R, Freeman ME.** Variations in the response of pituitary lactotrophs to oxytocin during the rat estrous cycle. *Endocrinology* 151: 1806–1813, 2010.
34. **Tabak J, Tomaiuolo M, Gonzalez-Iglesias AE, Milescu LS, Bertram R.** Fast-activating voltage- and calcium-dependent potassium (BK) conductance promotes bursting in pituitary cells: a dynamic clamp study. *J Neurosci* 31: 16855–16863, 2011.
35. **Tashjian AH, Yasumura Y, Levine L, Sato GH, Parker ML.** Establishment of clonal strains of rat pituitary tumor cells that secrete growth hormone. *Endocrinology* 82: 342–352, 1968.
36. **Thomas P, Surprenant A, Almers W.** Cytosolic Ca2+, exocytosis, and endocytosis in single melanotrophs of the rat pituitary. *Neuron* 5: 723–733, 1990.
37. **Thomas P, Wong JG, Lee AK, Almers W.** A low affinity Ca2+ receptor controls the final steps in peptide secretion from pituitary melanotrophs. *Neuron* 11: 93–104, 1993.
38. **Tse A, Hille B.** GnRH-induced Ca2+ oscillations and rhythmic hyperpolarizations of pituitary gonadotropes. *Science* 255: 462–464, 1992.
39. **Vardjan N, Jorgačevski J, Stenovec M, Kreft M, Zorec R.** Compound exocytosis in pituitary cells. *Ann NY Acad Sci* 1152: 63–75, 2009.
40. **Voets T.** Dissection of three Ca2+-dependent steps leading to secretion in chromaffin cells from mouse adrenal slices. *Neuron* 28: 537–545, 2000.
41. **Wildt L, Häusler A, Marshall G, Hutchison JS, Plant TM, Belchetz PE, Knobil E.** Frequency and amplitude of gonadotropin-releasing hormone stimulation and gonadotropin secretion in the rhesus monkey. *Endocrinology* 109: 376–385, 1981.
42. **Zorec R, Sikdar SK, Mason WT.** Increased cytosolic calcium stimulates exocytosis in bovine lactotrophs. Direct evidence from changes in membrane capacitance. *J Gen Physiol* 97: 473–497, 1991.